## H. Supplementary Figures

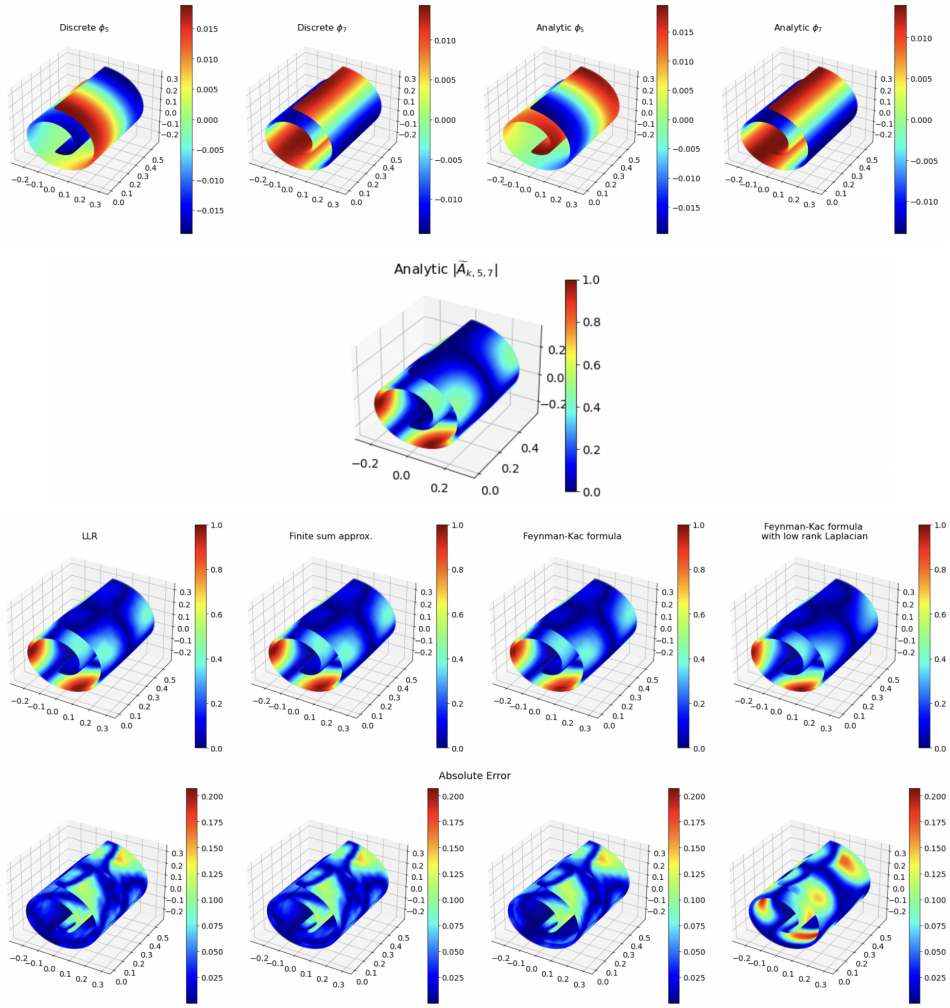


Figure 26: Comparison of different techniques to estimate $\widetilde{A}_{kij}$ on a Swiss Roll with no noise, where $i = 5$ and $j = 7$. (first row) Analytical eigenfunctions and the obtained discrete eigenvectors are shown. (second row) Analytical value of $|\widetilde{A}_{kij}|$ is shown. Note that LDLE depends on the absolute values of $\widetilde{A}_{kij}$. (third row) Estimation of $|\widetilde{A}_{kij}|$ are shown due to Local Linear Regression based approach (Cheng and Wu, 2013), finite sum approximation and Feynman-Kac formula based approaches as described in Section 3.2 and a variant of the latter which uses low rank (of 100) approximation of the graph Laplacian in Eq. (29). (fourth row) Absolute difference between the estimates and the analytical value. LLR, finite sum approx. and Feynman-Kac formula based approaches seem to perform slightly better.

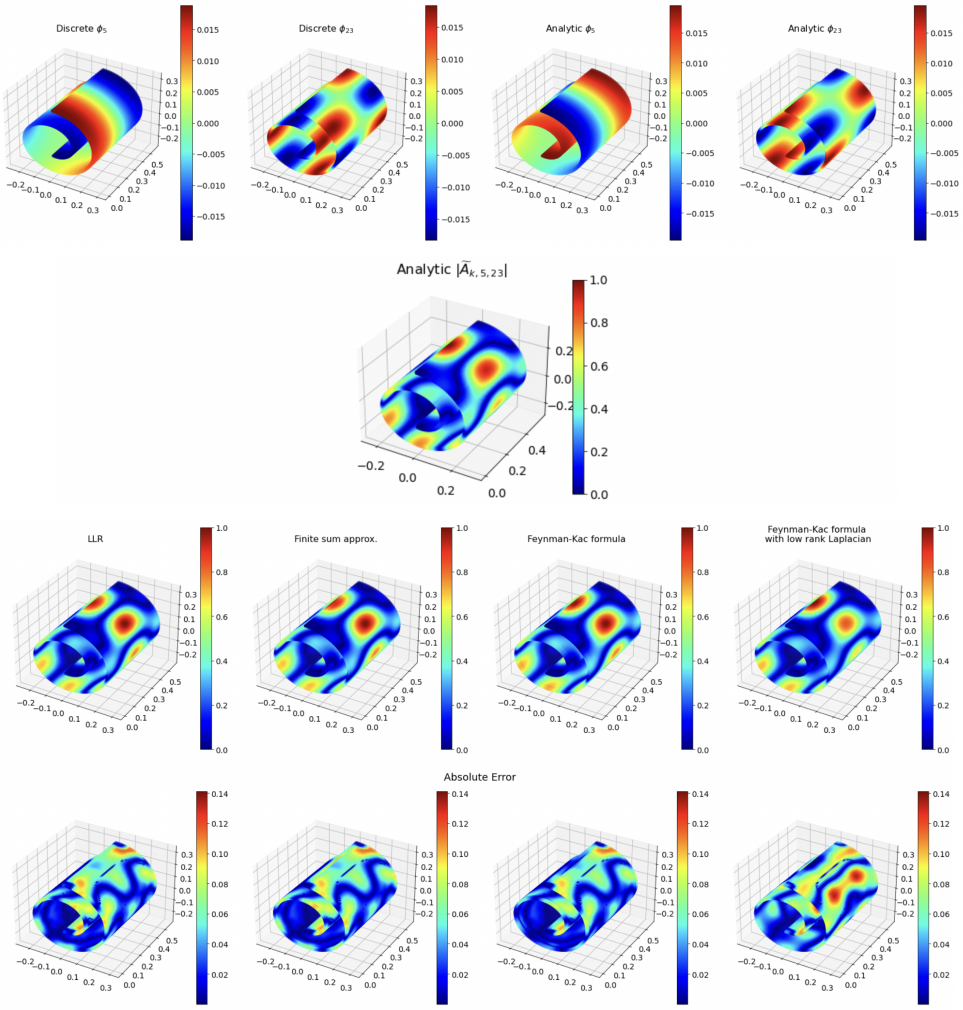


Figure 27: Comparison of different techniques to estimate $\widetilde{A}_{kij}$ on a Swiss Roll with no noise, where $i = 5$ and $j = 23$. (first row) Analytical eigenfunctions and the obtained discrete eigenvectors are shown. (second row) Analytical value of $|\widetilde{A}_{kij}|$ is shown. Note that LDLE depends on the absolute values of $\widetilde{A}_{kij}$. (third row) Estimation of $|\widetilde{A}_{kij}|$ are shown due to Local Linear Regression based approach (Cheng and Wu, 2013), finite sum approximation and Feynman-Kac formula based approaches as described in Section 3.2 and a variant of the latter which uses low rank (of 100) approximation of the graph Laplacian in Eq. (29). (fourth row) Absolute difference between the estimates and the analytical value. LLR, finite sum approx. and Feynman-Kac formula based approaches seem to perform slightly better.

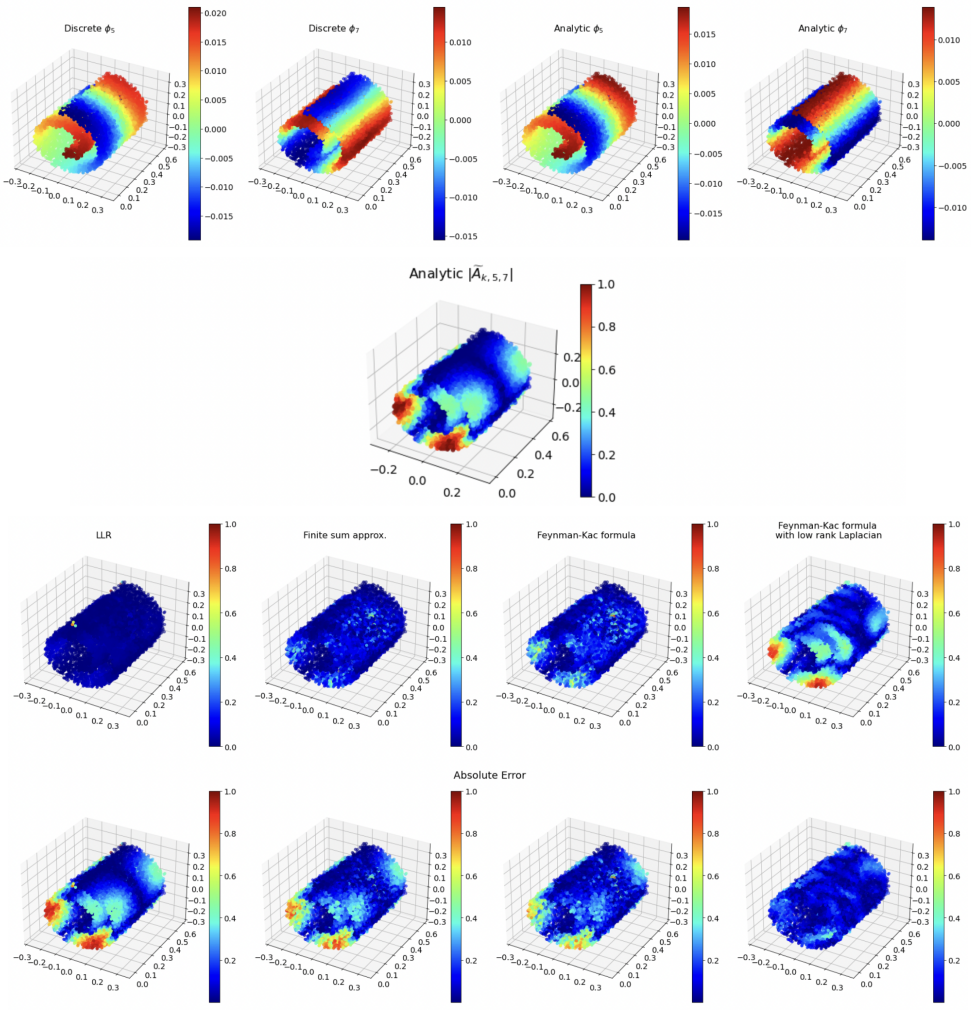


Figure 28: Comparison of different techniques to estimate $\widetilde{A}_{kij}$ on a Swiss Roll with Gaussian noise of variance $10^{-4}$, where $i = 5$ and $j = 7$. (first row) Analytical eigenfunctions obtained for the noiseless version of the Swiss Roll, and the obtained discrete eigenvectors are shown. (second row) Analytical value of $|\widetilde{A}_{kij}|$ is shown. Note that LDLE depends on the absolute values of $\widetilde{A}_{kij}$. (third row) Estimation of $|\widetilde{A}_{kij}|$ are shown due to Local Linear Regression based approach (Cheng and Wu, 2013), finite sum approximation and Feynman-Kac formula based approaches as described in Section 3.2 and a variant of the latter which uses low rank (of 100) approximation of the graph Laplacian in Eq. (29). (fourth row) Absolute difference between the estimates and the analytical value. The Feynman-Kac formula based approach which uses low rank approximation of $L$ seem to perform the best while the LLR based approach produced high error.

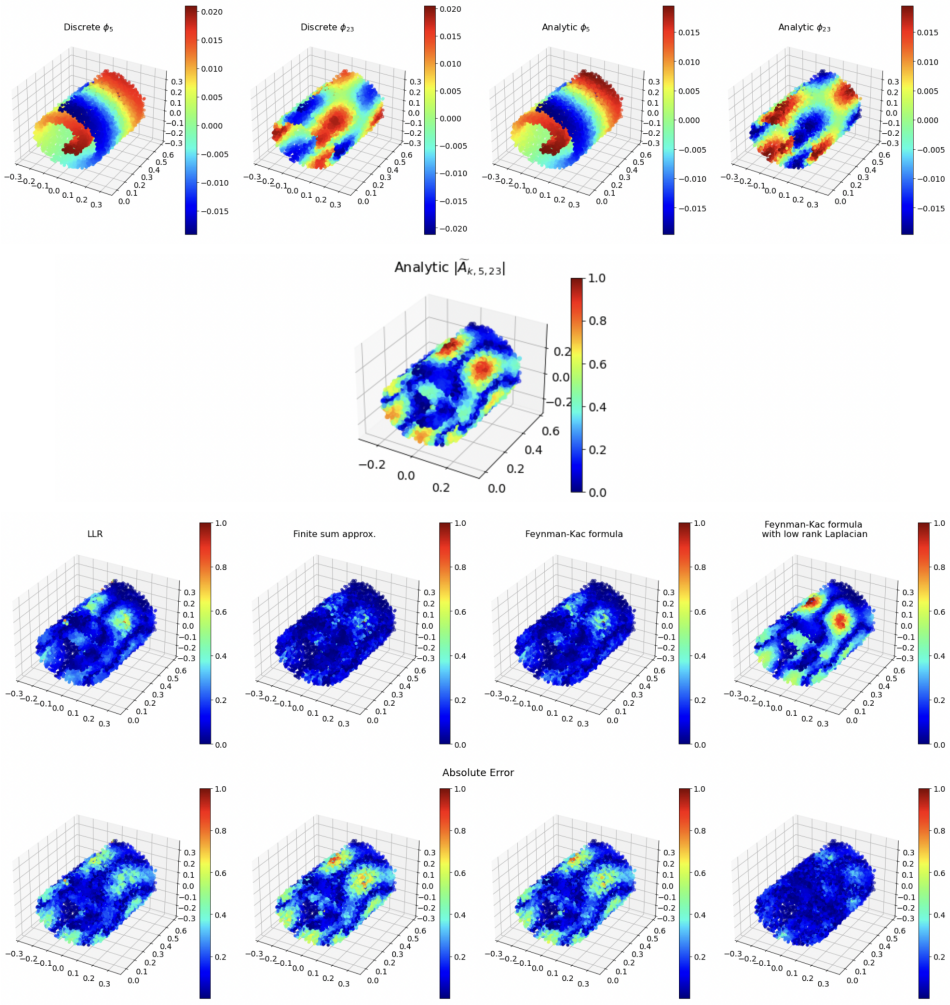


Figure 29: Comparison of different techniques to estimate $\widetilde{A}_{kij}$ on a Swiss Roll with Gaussian noise of variance $10^{-4}$, where $i = 5$ and $j = 23$. (first row) Analytical eigenfunctions obtained for the noiseless version of the Swiss Roll, and the obtained discrete eigenvectors are shown. (second row) Analytical value of $|\widetilde{A}_{kij}|$ is shown. Note that LDLE depends on the absolute values of $\widetilde{A}_{kij}$. (third row) Estimation of $|\widetilde{A}_{kij}|$ are shown due to Local Linear Regression based approach (Cheng and Wu, 2013), finite sum approximation and Feynman-Kac formula based approaches as described in Section 3.2 and a variant of the latter which uses low rank (of 100) approximation of the graph Laplacian in Eq. (29). (fourth row) Absolute difference between the estimates and the analytical value. The Feynman-Kac formula based approach which uses low rank approximation of $L$ seem to perform the best while the errors due to other three approaches are somewhat similar.

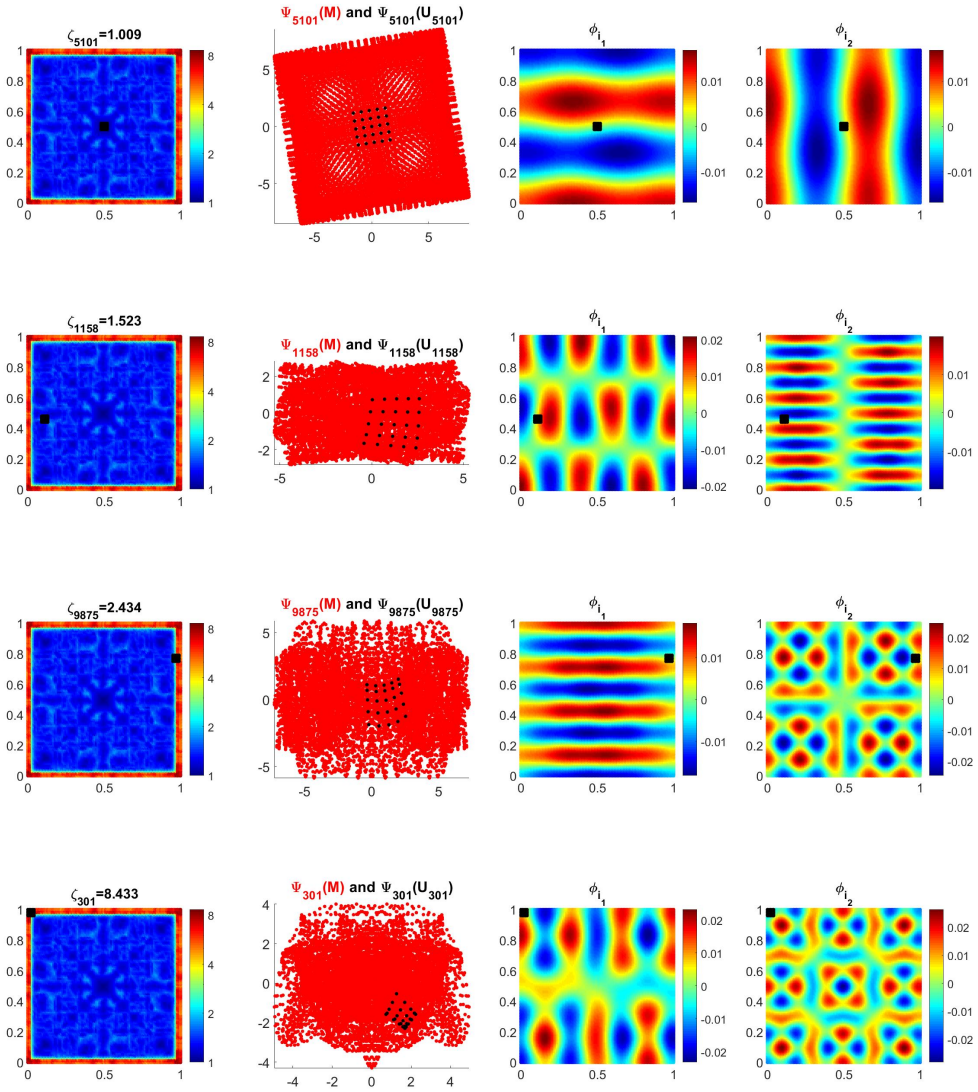


Figure 30: Visualization of the local views in the embedding space. (first column) Input square grid is shown. The points $x_k$ are colored by the distortion $\zeta_{kk}$ of the obtained local parameterizations $\Phi_k$ on the neighborhood $U_k$ surrounding them. A local view $U_{k_0}$ around $x_{k_0}$ for a fixed $k_0$ is also shown in black. (second column) The corresponding local view in the embedding space $\Phi_{k_0}(U_{k_0})$ is shown in black. Although of no significance to our algorithm, for visualization purpose, the embedding of the square due to $\Phi_{k_0}$, $\Phi_{k_0}(M)$, is shown in red. (third and fourth columns) The eigenvectors $\boldsymbol{\phi}_{i_1}$ and $\boldsymbol{\phi}_{i_2}$ chosen for the construction of $\Phi_{k_0}$ are shown. Points in $U_{k_0}$ are again colored in black. Note that the gradient of these eigenvectors are close to being orthogonal in the vicinity of $U_{k_0}$ and in particular, at $x_{k_0}$.

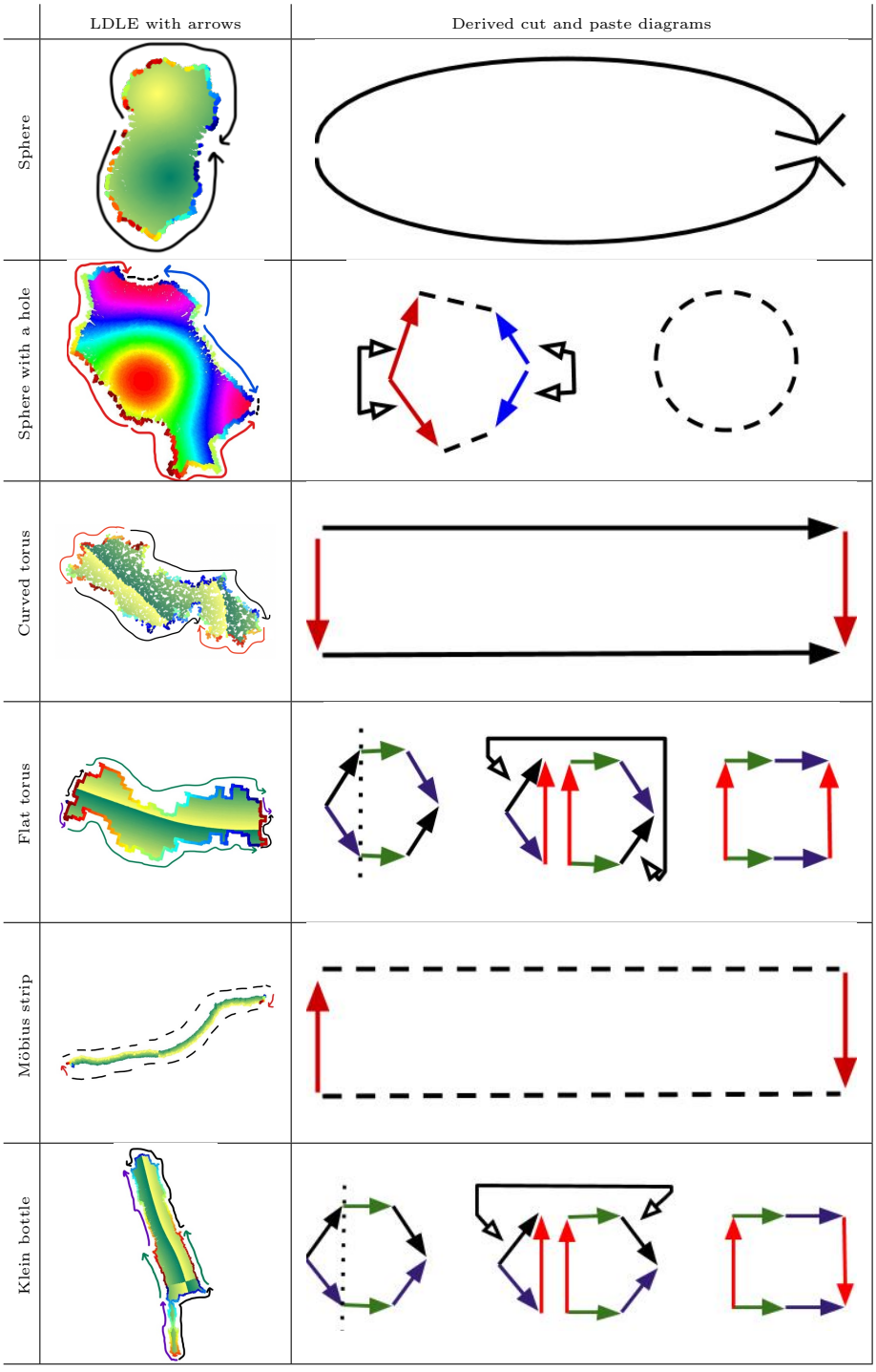


Figure 31: (Left) LDLE embedding with arrows drawn by tracing the colored boundary. (Right) Derived cut and paste diagrams to prove the correctness of the embedding. Pieces of the boundary represented by filled arrows of the same color are to be stitched together. Pieces of the boundary represented by black dashed lines are not to be stitched. Dotted lines and shallow arrows represent cut and paste instructions, respectively.

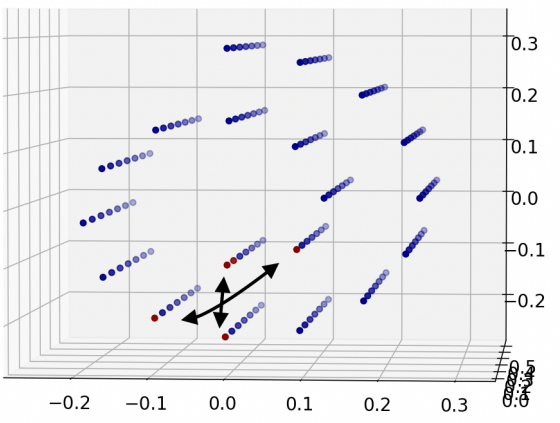


Figure 32: In Figure 18, for the case when RES = 10, certain points on the opposite sides of the gap between the Swiss Roll are neighbors in the ambient space. These points are shown in red.